

---

# PROXIMAL MEAN FIELD LEARNING IN SHALLOW NEURAL NETWORKS

---

Alexis M.H. Teter<sup>\*</sup>Iman Nodozi<sup>†</sup>Abhishek Halder<sup>‡</sup>

## ABSTRACT

Recent mean field interpretations of learning dynamics in over-parameterized neural networks offer theoretical insights on the empirical success of first order optimization algorithms in finding global minima of the nonconvex risk landscape. In this paper, we explore applying mean field learning dynamics as a computational algorithm, rather than as an analytical tool. Specifically, we design a Sinkhorn regularized proximal algorithm to approximate the distributional flow from the learning dynamics in the mean field regime over weighted point clouds. In this setting, a contractive fixed point recursion computes the time-varying weights, numerically realizing the interacting Wasserstein gradient flow of the parameter distribution supported over the neuronal ensemble. An appealing aspect of the proposed algorithm is that the measure-valued recursions allow meshless computation. We demonstrate the proposed computational framework of interacting weighted particle evolution on binary and multi-class classification. Our algorithm performs gradient descent of the free energy associated with the risk functional.

## 1 INTRODUCTION

While universal function approximation theorems for neural networks have been known for long [17], [4], such guarantees do not account the dynamics of the learning algorithms. Starting in 2018, several works [27], [15], [36], [39] pointed out that the first order learning dynamics for shallow (i.e., single hidden layer) neural networks in the infinite width (i.e., over-parameterization) limit leads to a nonlinear partial differential equation (PDE) that depends on a pair of advection and interaction potentials defined by both the loss function as well as the activation functions of the neural network. This can be thought of as a dynamical version of the universal approximation theorem. Remarkably, this PDE can be interpreted as the (infinite dimensional) gradient flow of the population risk w.r.t. the Wasserstein metric arising from the theory of optimal mass transport [42, 43].

As an analytic tool, this mean field Wasserstein gradient flow interpretation helps shed light on the convergence of first order learning dynamics in over-parameterized networks. In this work, we propose Wasserstein proximal recursions to realize the mean field learning dynamics as a meshless computational algorithm.

**Related work.** There exists a substantial literature on numerically implementing the Wasserstein gradient flows [2, 38] – both with grid [6, 13, 14, 32] and without grid [12, 21, 26], the latter more relevant for mean field learning context since the underlying parameter space is high dimensional. The proximal recursion we consider is closely related to the forward or backward discretization [20, 37] of the JKO (Jordan-Kinderlehrer-Otto) scheme [22].

To bypass numerical optimization over the manifold of measures or densities, recent works [1, 11, 28] propose using input convex neural networks [3] to perform the Wasserstein proximal time-stepping by learning the convex potentials [10] associated with the respective pushforward maps. To alleviate the computational difficulties in high dimensions, [8] propose replacing the Wasserstein distance with the sliced-Wasserstein distance [33] scaled by the ambient dimension.

**Contributions.** With respect to the related works mentioned above, the main contribution of the present work is that we propose a meshless Wasserstein proximal algorithm that directly implements the macroscopic learning dynamics in a fully connected shallow network by evolving population densities as *weighted* scattered particles. The explicit

---

<sup>\*</sup>Department of Applied Mathematics, University of California, Santa Cruz, amteter@ucsc.edu

<sup>†</sup>Department of Electrical and Computer Engineering, University of California, Santa Cruz, inodozi@ucsc.edu

<sup>‡</sup>Department of Applied Mathematics, University of California, Santa Cruz, ahalder@ucsc.edu

weight updates are done by solving a regularized dual ascent. The particles' location updates are done via non-local Euler-Maruyama. These two updates interact with each other, and together set up a discrete time-stepping scheme.

For specificity, we illustrate the proposed framework on two numerical experiments involving binary and multi-class classification with quadratic risk. The proposed methodology should be of broad interest to other problems such as the policy optimization [16, 45, 46], and the adversarial learning [18, 29].

**Notations and preliminaries.** We use the standard convention where the boldfaced lowercase letters denote vectors, boldfaced uppercase letters denote matrices, and non-boldfaced letters denote scalars. We use the symbols  $\nabla$  and  $\Delta$  to denote the Euclidean gradient and Laplacian operators, respectively. In case of potential confusion, we attach subscripts to these symbols to clarify the differential operator is taken w.r.t. which variable. The symbols  $\odot$ ,  $\oslash$ ,  $\exp$ , and  $\tanh$  denote *elementwise* multiplication, division, exponential, and hyperbolic tangent, respectively. Furthermore,  $\text{rand}$  and  $\text{randn}$  denote draw of the uniform and standard normal distributed random vector of appropriate dimension. In addition,  $\mathbf{1}$  represents a vector of ones of appropriate dimension.

The squared Wasserstein metric  $W_2$  (with standard Euclidean ground cost) between two probability measures  $\pi_1(d\mathbf{z}_1)$  and  $\pi_2(d\mathbf{z}_2)$  (or between the corresponding densities when the measures are absolutely continuous), where  $\mathbf{z}_1 \subseteq \mathcal{Z}_1$ ,  $\mathbf{z}_2 \subseteq \mathcal{Z}_2$ , is defined as

$$W_2^2(\pi_1, \pi_2) := \inf_{\pi \in \Pi(\pi_1, \pi_2)} \int_{\mathcal{Z}_1 \times \mathcal{Z}_2} \|\mathbf{z}_1 - \mathbf{z}_2\|_2^2 d\pi(\mathbf{z}_1, \mathbf{z}_2). \quad (1)$$

In (1),  $\Pi(\pi_1, \pi_2)$  denotes the collection of joint measures (couplings) with finite second moments, whose first marginal is  $\pi_1$ , and the second marginal is  $\pi_2$ .

## 2 FROM EMPIRICAL RISK MINIMIZATION TO PROXIMAL MEAN FIELD LEARNING

**Empirical Risk Minimization.** We consider a supervised learning problem where the dataset comprises of the features  $\mathbf{x} \in \mathcal{X} \subseteq \mathbb{R}^{n_x}$ , and the labels  $y \in \mathcal{Y} \subseteq \mathbb{R}$ , i.e., the samples of the dataset are tuples of the form

$$(\mathbf{x}, y) \in \mathcal{X} \times \mathcal{Y} \subseteq \mathbb{R}^{n_x} \times \mathbb{R}.$$

The objective of the supervised learning problem is to find the parameter vector  $\boldsymbol{\theta} \in \mathbb{R}^p$  such that  $y \approx f(\mathbf{x}, \boldsymbol{\theta})$  where  $f$  is some function class parameterized by  $\boldsymbol{\theta}$ . In other words,  $f$  maps from the feature space  $\mathcal{X}$  to the label space  $\mathcal{Y}$ . To this end, we consider a shallow neural network with single hidden layer having  $n_H$  neurons. Then, the parameterized function  $f$  admits representation

$$f(\mathbf{x}, \boldsymbol{\theta}) := \frac{1}{n_H} \sum_{i=1}^{n_H} \Phi(\mathbf{x}, \boldsymbol{\theta}_i), \quad (2)$$

where  $\Phi(\mathbf{x}, \boldsymbol{\theta}_i) := a_i \sigma(\langle \mathbf{w}_i, \mathbf{x} \rangle + b_i)$  for all  $i \in [n_H] := \{1, 2, \dots, n_H\}$ , and  $\sigma(\cdot)$  is a smooth activation function. The parameters  $a_i$ ,  $\mathbf{w}_i$  and  $b_i$  are the scaling, weight and bias of the  $i^{\text{th}}$  hidden neuron, respectively, and together comprise the specific parameter realization  $\boldsymbol{\theta}_i \in \mathbb{R}^p$ ,  $i \in [n_H]$ .

We stack the parameter vectors of all hidden neurons as

$$\bar{\boldsymbol{\theta}} := \begin{pmatrix} \boldsymbol{\theta}_1 \\ \boldsymbol{\theta}_2 \\ \vdots \\ \boldsymbol{\theta}_{n_H} \end{pmatrix} \in \mathbb{R}^{pn_H}, \quad (3)$$

and consider minimizing the following quadratic loss:

$$l(y, \mathbf{x}, \bar{\boldsymbol{\theta}}) \equiv l(y, f(\mathbf{x}, \bar{\boldsymbol{\theta}})) := \underbrace{(y - f(\mathbf{x}, \bar{\boldsymbol{\theta}}))^2}_{\text{quadratic loss}}. \quad (4)$$

We suppose that the training data follows the joint probability distribution  $\gamma$ , i.e.,  $(\mathbf{x}, y) \sim \gamma$ . Define the *population risk*  $R$  as the expected loss given by

$$R(f) := \mathbb{E}_{(\mathbf{x}, y) \sim \gamma} [l(y, \mathbf{x}, \bar{\boldsymbol{\theta}})]. \quad (5)$$

In practice,  $\gamma$  is unknown, so we approximate the population risk with the *empirical risk*

$$R(f) \approx \frac{1}{n_{\text{data}}} \sum_{j=1}^{n_{\text{data}}} l(y_j, \mathbf{x}_j, \bar{\boldsymbol{\theta}}) \quad (6)$$

where  $n_{\text{data}}$  is the number of data samples. Then, the supervised learning problem reduces to the empirical risk minimization problem

$$\min_{\bar{\theta} \in \mathbb{R}^{p_{\text{H}}}} R(f). \quad (7)$$

Problem (7) is a large but finite dimensional optimization problem that is nonconvex in the decision variable  $\bar{\theta}$ . The standard approach to solve the same is to employ first or second order search algorithms such as the variants of stochastic gradient descent (SGD), ADAM [24].

**Mean Field Limit.** The mean field limit concerns with a continuum of hidden layer neuronal population by letting  $n_{\text{H}} \rightarrow \infty$ . Then, we view (2) as the empirical average associated with the ensemble average

$$f_{\text{MeanField}} := \int_{\mathbb{R}^p} \Phi(\mathbf{x}, \boldsymbol{\theta}) \underbrace{d\mu(\boldsymbol{\theta})}_{\text{hidden neuronal population mass}} = \mathbb{E}_{\boldsymbol{\theta}}[\Phi(\mathbf{x}, \boldsymbol{\theta})], \quad (8)$$

where  $\mu$  denotes the joint population measure supported on the hidden neuronal parameter space in  $\mathbb{R}^p$ . Assuming the absolute continuity of  $\mu$  for all times, we write  $d\mu(\boldsymbol{\theta}) = \rho(\boldsymbol{\theta})d\boldsymbol{\theta}$  where  $\rho$  denotes the joint population density function (PDF). Thus, the risk functional  $R$ , now viewed as a function of the joint PDF  $\rho$ , takes the form

$$\begin{aligned} F(\rho) &:= R(f_{\text{MeanField}}(\mathbf{x}, \rho)) = \mathbb{E}_{(\mathbf{x}, y)} \left( y - \int_{\mathbb{R}^p} \Phi(\mathbf{x}, \boldsymbol{\theta}) \rho(\boldsymbol{\theta}) d\boldsymbol{\theta} \right)^2 \\ &= F_0 + \int_{\mathbb{R}^p} V(\boldsymbol{\theta}) \rho(\boldsymbol{\theta}) d\boldsymbol{\theta} + \int_{\mathbb{R}^{2p}} U(\boldsymbol{\theta}, \tilde{\boldsymbol{\theta}}) \rho(\boldsymbol{\theta}) \rho(\tilde{\boldsymbol{\theta}}) d\boldsymbol{\theta} d\tilde{\boldsymbol{\theta}}, \end{aligned} \quad (9)$$

where

$$\begin{aligned} F_0 &:= \mathbb{E}_{(\mathbf{x}, y)} [y^2], \\ V(\boldsymbol{\theta}) &:= \mathbb{E}_{(\mathbf{x}, y)} [-2y\Phi(\mathbf{x}, \boldsymbol{\theta})], \\ U(\boldsymbol{\theta}, \tilde{\boldsymbol{\theta}}) &:= \mathbb{E}_{(\mathbf{x}, y)} [\Phi(\mathbf{x}, \boldsymbol{\theta})\Phi(\mathbf{x}, \tilde{\boldsymbol{\theta}})]. \end{aligned} \quad (10)$$

Therefore, the supervised learning problem, in this mean field limit, becomes an infinite dimensional variational problem:

$$\min_{\rho} F(\rho), \quad (11)$$

where  $F$  is a sum of three functionals. The first summand  $F_0$  is independent of  $\rho$ . The second summand is a potential energy given by expected value of “drift potential”  $V$ , and is linear in  $\rho$ . The last summand is a bilinear interaction energy involving an “interaction potential”  $U$ , and is nonlinear in  $\rho$ .

The main result in [27] was that using first order SGD learning dynamics induces a gradient flow of the functional  $F$  w.r.t. the 2-Wasserstein metric  $W_2$ , i.e., the mean field learning dynamics results in a joint PDF trajectory  $\rho(t, \boldsymbol{\theta})$ . Then, the minimizer in (11) can be obtained from the large  $t$  limit of the following nonlinear PDE:

$$\frac{\partial \rho}{\partial t} = -\nabla^{W_2} F(\rho), \quad (12)$$

where the 2-Wasserstein gradient [43, Ch. 9.1] [2, Ch. 8] of  $F$  is

$$\nabla^{W_2} F(\rho) := -\nabla \cdot \left( \rho \nabla \frac{\delta F}{\delta \rho} \right),$$

and  $\frac{\delta}{\delta \rho}$  denotes the functional derivative w.r.t.  $\rho$ .

In particular, [27] considered the regularized risk functional<sup>4</sup>

$$F_{\beta}(\rho) := F(\rho) + \beta^{-1} \int_{\mathbb{R}^p} \rho \log \rho d\boldsymbol{\theta}, \quad \beta > 0, \quad (13)$$

by adding a strictly convex regularizer (scaled negative entropy) to the unregularized risk  $F$ . In that case, the sample path dynamics corresponding to the macroscopic dynamics (12) precisely becomes the noisy SGD:

$$d\boldsymbol{\theta} = -\nabla_{\boldsymbol{\theta}} \left( V(\boldsymbol{\theta}) + \int_{\mathbb{R}^p} U(\boldsymbol{\theta}, \tilde{\boldsymbol{\theta}}) \rho(\tilde{\boldsymbol{\theta}}) d\tilde{\boldsymbol{\theta}} \right) dt + \sqrt{2\beta^{-1}} d\mathbf{w}, \quad \boldsymbol{\theta}(t=0) \sim \rho_0, \quad (14)$$

<sup>4</sup>The parameter  $\beta > 0$  is referred to as the inverse temperature.

where  $\mathbf{w}$  is the standard Wiener process in  $\mathbb{R}^p$ , and the random initial condition  $\boldsymbol{\theta}(t = 0)$  follows the law of a suitable PDF  $\rho_0$  supported over  $\mathbb{R}^p$ .

In this regularized case, (12) results in the following nonlinear PDE initial value problem (IVP):

$$\frac{\partial \rho}{\partial t} = \nabla_{\boldsymbol{\theta}} \cdot \left( \rho \left( V(\boldsymbol{\theta}) + \int_{\mathbb{R}^p} U(\boldsymbol{\theta}, \tilde{\boldsymbol{\theta}}) \rho(\tilde{\boldsymbol{\theta}}) d\tilde{\boldsymbol{\theta}} \right) \right) + \beta^{-1} \Delta_{\boldsymbol{\theta}} \rho, \quad \rho(t = 0, \boldsymbol{\theta}) = \rho_0. \quad (15)$$

In other words, the noisy SGD induces evolution of a PDF-valued trajectory governed by the advection, nonlocal interaction and diffusion—the latter originating from regularization. Notice that a large value of  $\beta > 0$  implies a small entropic regularization in (13), hence a small additive process noise in (14), and consequently, a small diffusion term in the PDE (15).

The regularized risk functional  $F_{\beta}$  in (13) can be interpreted as a free energy wherein  $F$  contributes a sum of the advection potential energy and interaction energy. The term  $\beta^{-1} \int_{\mathbb{R}^p} \rho \log \rho d\boldsymbol{\theta}$  contributes an internal energy due to the noisy fluctuations induced by the additive Wiener process noise  $\sqrt{2\beta^{-1}} d\mathbf{w}$  in (14).

In [27], asymptotic guarantees were obtained for the solution of (15) to converge to the minimizer of  $F_{\beta}$ . Our idea outlined next, is to solve the minimization of  $F_{\beta}$  using measure-valued proximal recursions.

**Proximal Mean Field Learning.** For numerically computing the solution of the PDE IVP (15), we propose proximal recursions over  $\mathcal{P}_2(\mathbb{R}^p)$ , defined as the manifold of joint PDFs supported over  $\mathbb{R}^p$  having finite second moments. Proximal updates generalize the concept of gradient steps, and are of significant interest in both finite and infinite dimensional optimization [5, 7, 30, 34, 35, 40].

Specifically, we propose recursions over discrete time  $t_{k-1} := (k-1)h$  where the index  $k \in \mathbb{N}$ , and  $h > 0$  is a constant time step-size. Leveraging that (15) describes gradient flow of the functional  $F_{\beta}$  w.r.t.  $W_2$  distance metric, the associated proximal recursion is of the form

$$\varrho_k = \text{prox}_{hF_{\beta}}^{W_2}(\varrho_{k-1}) := \arg \inf_{\varrho \in \mathcal{P}_2(\mathbb{R}^p)} \frac{1}{2} (W_2(\varrho, \varrho_{k-1}))^2 + hF_{\beta}(\varrho) \quad (16)$$

where  $\varrho_{k-1}(\cdot) := \varrho(\cdot, t_{k-1})$ , and  $\varrho_0 \equiv \rho_0$ .

To account for the nonconvex bilinear term appearing in (13), following [6, Sec. 4], we employ the approximation:  $\int_{\mathbb{R}^{2p}} U(\boldsymbol{\theta}, \tilde{\boldsymbol{\theta}}) \varrho(\boldsymbol{\theta}) \varrho(\tilde{\boldsymbol{\theta}}) d\boldsymbol{\theta} d\tilde{\boldsymbol{\theta}} \approx \int_{\mathbb{R}^{2p}} U(\boldsymbol{\theta}, \tilde{\boldsymbol{\theta}}) \varrho(\boldsymbol{\theta}) \varrho_{k-1}(\tilde{\boldsymbol{\theta}}) d\boldsymbol{\theta} d\tilde{\boldsymbol{\theta}}$  for all  $k \in \mathbb{N}$ . We refer to the resulting approximation of  $F_{\beta}$  as  $\hat{F}_{\beta}$ , i.e.,

$$\hat{F}_{\beta}(\varrho, \varrho_{k-1}) := \int_{\mathbb{R}^p} \left( F_0 + V(\boldsymbol{\theta}) \left( \int_{\mathbb{R}^p} U(\boldsymbol{\theta}, \tilde{\boldsymbol{\theta}}) \varrho_{k-1}(\tilde{\boldsymbol{\theta}}) d\tilde{\boldsymbol{\theta}} \right) + \beta^{-1} \log \varrho(\boldsymbol{\theta}) \right) \varrho(\boldsymbol{\theta}) d\boldsymbol{\theta}.$$

Notice in particular that  $\hat{F}_{\beta}$  depends on both  $\varrho, \varrho_{k-1}, k \in \mathbb{N}$ . Consequently, this approximation results in a semi-implicit variant of (16), given by

$$\varrho_k := \arg \inf_{\varrho \in \mathcal{P}_2(\mathbb{R}^p)} \frac{1}{2} (W_2(\varrho, \varrho_{k-1}))^2 + h\hat{F}_{\beta}(\varrho, \varrho_{k-1}). \quad (17)$$

We have the following consistency guarantee among the solution of the PDE IVP (15) and that of the variational recursions (17).

**Theorem 1.** *Consider the regularized risk functional (13) wherein  $F$  is given by (9)-(10). Let  $\rho(t, \boldsymbol{\theta})$  solve the IVP (15), and let  $\{\varrho_{k-1}\}_{k \in \mathbb{N}}$  be the sequence of functions generated by (17) with  $\varrho_0 \equiv \rho_0$ . Then*

$$\varrho_k(h, \boldsymbol{\theta}) \xrightarrow{h \downarrow 0} \rho(t = kh, \boldsymbol{\theta}) \text{ in } L^1(\mathbb{R}^p), \quad k \in \mathbb{N}. \quad (18)$$

We next detail the proposed algorithmic approach to numerically solve (17).

### 3 Proximal Algorithm

The overall workflow of our proposed proximal mean field learning framework is shown in Fig. 1. We generate  $N$  samples from the known initial joint PDF  $\varrho_0$  and store them as a weighted point cloud  $\{\boldsymbol{\theta}_0^i, \varrho_0^i\}_{i=1}^N$ . Here,  $\varrho_0^i := \varrho_0(\boldsymbol{\theta}_0^i)$  for all  $i \in [N]$ . In other words, the weights of the samples are the joint PDF values evaluated at those samples.

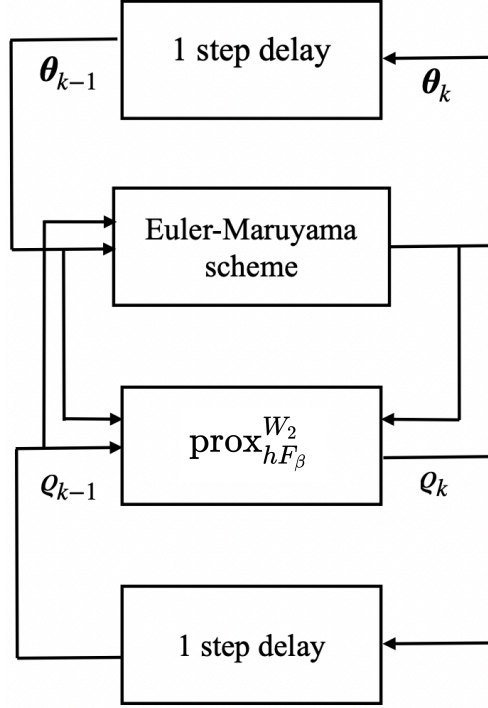


Figure 1: Schematic of the proposed proximal algorithm for mean field learning by updating scattered point cloud  $\{\theta_{k-1}^i, \varrho_{k-1}^i\}_{i=1}^N$  for  $k \in \mathbb{N}$ . The location of the points  $\{\theta_{k-1}^i\}_{i=1}^N$  are updated via the Euler-Maruyama scheme; the corresponding probability weights are computed via proximal updates.

For each  $k \in \mathbb{N}$ , the weighted point clouds  $\{\theta_k^i, \varrho_k^i\}_{i=1}^N$  are updated through the two-step process detailed in Algorithm 1, PROXLEARN. We emphasize here that proposed PROXLEARN algorithm updates both the parameter sample locations  $\theta_k^i$  as well as the joint PDF values  $\varrho_k^i$  evaluated at those locations without gridding the parameter space.

The PROXLEARN procedure as outlined here will be applied in Sec. 4. In Sec. 5, we will detail additional modifications of PROXLEARN to showcase its flexibility.

Required inputs of PROXLEARN are the inverse temperature  $\beta$ , the time step-size  $h$ , a regularization parameter  $\varepsilon$ , and the number of samples  $N$ . Additionally required inputs are the training feature data

$$\mathbf{X} := [\mathbf{x}_1 \dots \mathbf{x}_{n_{\text{data}}}]^\top \in \mathbb{R}^{n_{\text{data}} \times n_x},$$

the corresponding training labels

$$\mathbf{y} := [y_1 \dots y_{n_{\text{data}}}]^\top \in \mathbb{R}^{n_{\text{data}}},$$

as well the weighted point cloud  $\{\theta_{k-1}^i, \varrho_{k-1}^i\}_{i=1}^N$  for each  $k \in \mathbb{N}$ . Furthermore, PROXLEARN requires two internal parameters as user input: the numerical tolerance  $\delta$ , and the maximum number of iterations  $L$ .

For convenience, let

$$\Theta_{k-1} := \begin{pmatrix} (\theta_{k-1}^1)^\top \\ (\theta_{k-1}^2)^\top \\ \vdots \\ (\theta_{k-1}^N)^\top \end{pmatrix} \in \mathbb{R}^{N \times p}, \quad (19)$$

$$\varrho_{k-1} := \begin{pmatrix} \varrho_{k-1}^1 \\ \varrho_{k-1}^2 \\ \vdots \\ \varrho_{k-1}^N \end{pmatrix} \in \mathbb{R}_{>0}^N, \quad k \in \mathbb{N}. \quad (20)$$

**Algorithm 1** Proximal Algorithm

---

```

1: procedure PROXLEARN( $\mathbf{q}_{k-1}, \mathbf{\Theta}_{k-1}, \beta, h, \varepsilon, N, \mathbf{X}, \mathbf{y}, \delta, L$ )
2:    $\mathbf{v}_{k-1}, \mathbf{U}_{k-1}, \mathbf{\Theta}_k \leftarrow \text{EULERMARUYAMA}(h, \beta, \mathbf{\Theta}_{k-1}, \mathbf{X}, \mathbf{y}, \mathbf{q}_{k-1})$ 
3:    $C_k(i, j) \leftarrow \left\| \boldsymbol{\theta}_k^i - \boldsymbol{\theta}_{k-1}^j \right\|_2^2$ 
4:    $\Gamma_k \leftarrow \exp(-C_k/2\varepsilon)$ 
5:    $\boldsymbol{\xi}_{k-1} \leftarrow \exp(-\beta \mathbf{v}_{k-1} - \beta \mathbf{U}_{k-1} \mathbf{q}_{k-1} - \mathbf{1})$ 
6:    $\mathbf{z}_0 \leftarrow \text{rand}_{N \times 1}$ 
7:    $\mathbf{z} \leftarrow [\mathbf{z}_0, \mathbf{0}_{N \times (L-1)}]$ 
8:    $\mathbf{q} \leftarrow [\mathbf{q}_{k-1} \odot (\Gamma_k \mathbf{z}_0), \mathbf{0}_{N \times (L-1)}]$ 
9:    $\ell = 1$ 
10:  while  $\ell \leq L$  do
11:     $\mathbf{z}(:, \ell + 1) \leftarrow (\boldsymbol{\xi}_{k-1} \odot (\Gamma_k^\top \mathbf{q}(:, \ell)))^{\frac{1}{1+\beta\varepsilon/h}}$ 
12:     $\mathbf{q}(:, \ell + 1) \leftarrow \mathbf{q}_{k-1} \odot (\Gamma_k \mathbf{z}(:, \ell + 1))$ 
13:    if  $\|\mathbf{q}(:, \ell + 1) - \mathbf{q}(:, \ell)\| < \delta$  and  $\|\mathbf{z}(:, \ell + 1) - \mathbf{z}(:, \ell)\| < \delta$  then
14:      Break
15:    else
16:       $\ell \leftarrow \ell + 1$ 
17:    end if
18:  end while
19:  return  $\mathbf{q}_k \leftarrow \mathbf{z}(:, \ell) \odot (\Gamma_k^\top \mathbf{q}(:, \ell))$ 
20: end procedure

```

---

**Algorithm 2** Euler-Maruyama Algorithm

---

```

1: procedure EULERMARUYAMA( $h, \beta, \mathbf{\Theta}_{k-1}, \mathbf{X}, \mathbf{y}, \mathbf{q}_{k-1}$ )
2:    $\mathbf{P}_{k-1} \leftarrow \Phi(\mathbf{\Theta}_{k-1}, \mathbf{X})$ 
3:    $\mathbf{U}_{k-1} \leftarrow 1/n_{\text{data}} \mathbf{P}_{k-1} \mathbf{P}_{k-1}^\top$ 
4:    $\mathbf{u}_{k-1} \leftarrow \mathbf{U}_{k-1} \mathbf{q}_{k-1}$ 
5:    $\mathbf{v}_{k-1} \leftarrow -2/n_{\text{data}} \mathbf{P}_{k-1} \mathbf{y}$ 
6:    $\mathbf{D} \leftarrow \text{BACKWARD}(\mathbf{u}_{k-1} + \mathbf{v}_{k-1})$ 
7:    $\mathbf{G} \leftarrow \sqrt{2h/\beta} \times \text{randn}_{N \times p}$ 
8:    $\mathbf{\Theta}_k \leftarrow \mathbf{\Theta}_{k-1} + h \times \mathbf{D} + \mathbf{G}$ 
9: end procedure

```

---

In line 2 of Algorithm 1, PROXLEARN updates the locations of the parameter vector samples  $\boldsymbol{\theta}_k^i$  in  $\mathbb{R}^p$  via Algorithm 2, EULERMARUYAMA. This location update takes the form:

$$\boldsymbol{\theta}_k^i = \boldsymbol{\theta}_{k-1}^i - h \nabla (V(\boldsymbol{\theta}_{k-1}^i) + \omega(\boldsymbol{\theta}_{k-1}^i)) + \sqrt{2\beta^{-1}} (\mathbf{w}_k^i - \mathbf{w}_{k-1}^i), \quad (21)$$

where  $\omega(\cdot) := \int U(\cdot, \tilde{\boldsymbol{\theta}}) \varrho(\tilde{\boldsymbol{\theta}}) d\tilde{\boldsymbol{\theta}}$ , and  $\mathbf{w}_{k-1}^i := \mathbf{w}^i(t = (k-1)h)$ ,  $\forall k \in \mathbb{N}$ .

To perform this update, EULERMARUYAMA constructs a matrix  $\mathbf{P}_{k-1}$  whose (i,j)th element is  $\mathbf{P}_{k-1}(i, j) = \Phi(\mathbf{x}_j, \boldsymbol{\theta}_{k-1}^i)$ . From  $\mathbf{P}_{k-1}$ , we construct  $\mathbf{v}_{k-1}$  and  $\mathbf{U}_{k-1}$  as in lines 3 and 5. In line 6 of Algorithm 2, EULERMARUYAMA uses the automatic differentiation module of the PyTorch Library, BACKWARD [31], to calculate the gradients needed to update  $\mathbf{\Theta}_{k-1}$  to  $\mathbf{\Theta}_k$ , where  $k \in \mathbb{N}$ .

Once  $\mathbf{\Theta}_k$ ,  $\mathbf{v}_{k-1}$ , and  $\mathbf{U}_{k-1}$  have been constructed via EULERMARUYAMA, then PROXLEARN maps the  $N \times 1$  vector  $\mathbf{q}_{k-1}$  to the proximal update  $\mathbf{q}_k$ . For the detailed derivation of PROXLEARN following Sinkhorn regularization and dualization, and its contractive convergence guarantee, we refer the readers to the Supplementary Material.

We next illustrate the application of PROXLEARN for binary and multi-class classification.

## 4 CASE STUDY: BINARY CLASSIFICATION

This numerical case study is performed on a PC with 3.4 GHz 6-Core Intel Core i5 processor, and 8 GB RAM. For runtime improvement, we use a Jetson TX2 having a NVIDIA Pascal GPU with 256 CUDA cores, 64-bit NVIDIA Denver and ARM Cortex-A57 CPUs.

$\beta$	Estimate #1	Estimate #2
0.03	91.17%	92.35%
0.05	92.94%	92.94%
0.07	78.23%	92.94%

Table 1: Classification accuracy of the proposed computational framework for the WDBC dataset with different values of the inverse temperature  $\beta$ .

**WDBC Data Set.** We apply the proposed algorithm to perform a binary classification on the Wisconsin Diagnostic Breast Cancer (henceforth, WDBC) data set available at the UC Irvine machine learning repository [19]. This data set consists of the data of scans from 569 patients. There are  $n_x = 30$  features from each scan. Scans are classified as “benign” (which we label as  $-1$ ) or “malignant” (labeled as  $+1$ ).

In (2), we define  $\Phi(\mathbf{x}, \boldsymbol{\theta}_{k-1}^i) := a_{k-1}^i \tanh(\langle \mathbf{w}_{k-1}^i, \mathbf{x} \rangle + b_{k-1}^i)$  for all  $i \in [N]$  after  $(k-1)$  updates. The parameters  $a_{k-1}^i$ ,  $\mathbf{w}_{k-1}^i$  and  $b_{k-1}^i$  are the scaling, weight and bias of the  $i^{\text{th}}$  sample after  $(k-1)$  updates, respectively. Letting  $p := n_x + 2$ , the parameter vector of the  $i^{\text{th}}$  sample after  $(k-1)$  updates is

$$\boldsymbol{\theta}_{k-1}^i := \begin{pmatrix} a_{k-1}^i \\ b_{k-1}^i \\ \mathbf{w}_{k-1}^i \end{pmatrix} \in \mathbb{R}^p, \quad \forall i \in [N].$$

We set  $\varrho_0 \equiv \text{Unif}([0.9, 1.1] \times [-0.1, 0.1] \times [-1, 1]^{n_x})$ , a uniform joint PDF supported over  $n_p = n_x + 2 = 32$  dimensional mean field parameter space.

We use 70% of the entire data set as training data. As discussed in Sec. 3, we learn the mean field parameter distribution via weighted scattered point cloud evolution using PROXLEARN. We then use the confusion matrix method [44] to evaluate the accuracy of the obtained model over the test data, which is the remaining 30% of the full data set, containing  $n_{\text{test}}$  points.

For each test point  $\mathbf{x}_{\text{test}} \in \mathbb{R}^{n_x}$ , we construct

$$\boldsymbol{\varphi}(\mathbf{x}_{\text{test}}) := \begin{pmatrix} \Phi(\mathbf{x}_{\text{test}}, \boldsymbol{\theta}_{k-1}^1) \\ \Phi(\mathbf{x}_{\text{test}}, \boldsymbol{\theta}_{k-1}^2) \\ \vdots \\ \Phi(\mathbf{x}_{\text{test}}, \boldsymbol{\theta}_{k-1}^N) \end{pmatrix} \in \mathbb{R}^N$$

where  $\boldsymbol{\theta}_{k-1}^i$  is obtained from the training process. We estimate  $f_{\text{MeanField}}$  in (8) in two ways. First, we estimate  $f_{\text{MeanField}}$  as a sample average of the elements of  $\boldsymbol{\varphi}$ . Second, we estimate  $f_{\text{MeanField}}$  by numerically approximating the integral in (8) using the propagated samples  $\{\boldsymbol{\theta}_{k-1}^i, \varrho_{k-1}^i\}_{i=1}^N$  for  $k \in \mathbb{N}$ . We refer to these as the “estimate #1” and “estimate #2”, respectively. While the first estimate is an empirical average, the second uses the weights  $\{\varrho_{k-1}^i\}_{i=1}^N$  obtained from the proposed proximal algorithm. The  $f_{\text{MeanField}}$  estimates thus obtained, are then passed through the SOFTMAX (for estimate #1) and ARGMAX (for estimate #2) functions, respectively, to produce the predicted labels.

**Numerical Experiments.** We set the number of samples  $N = 1000$ , numerical tolerance  $\delta = 10^{-3}$ , the maximum number of iterations  $L = 300$ , and the regularizing parameter  $\varepsilon = 1$ . Additionally, we set the time step to  $h = 10^{-3}$ . We run the simulation for different values of the inverse temperature  $\beta$ , and list the corresponding classification accuracy in Table 1. Estimate #2, the ensemble average using proximal updates, produces more accurate results, whereas estimate #1, the empirical average, is found to be more sensitive on the inverse temperature  $\beta$ .

For each fixed  $\beta$ , we perform  $10^6$  proximal recursions incurring approx. 33 hours of computational time. Fig. 2 compares the predicted labels with the actual labels for the two estimation methods. Fig. 3a shows the risk functional, computed as the averaged loss over the test data using each of the two estimates described above.

**Runtime Improvements.** To improve the runtime of our algorithm, we run our code on a Jetson TX2 module, converting data and variables to PyTorch variables.

We begin calculations in Float32, switching to Float64 only when needed to avoid not-a-number (NaN) errors. This switch typically occurs after  $2 \times 10^5$  to  $3 \times 10^5$  iterations. As shown in Table 2, we train the neural network to a comparable accuracy in only  $2.5 \times 10^5$  iterations. The new runtime is around 6% of the original runtime for the CPU-based computation. Fig. 3b shows the risk functional calculated via this updated code. We parallelize these calculations, taking advantage of the GPU capacity of the Jetson TX2.

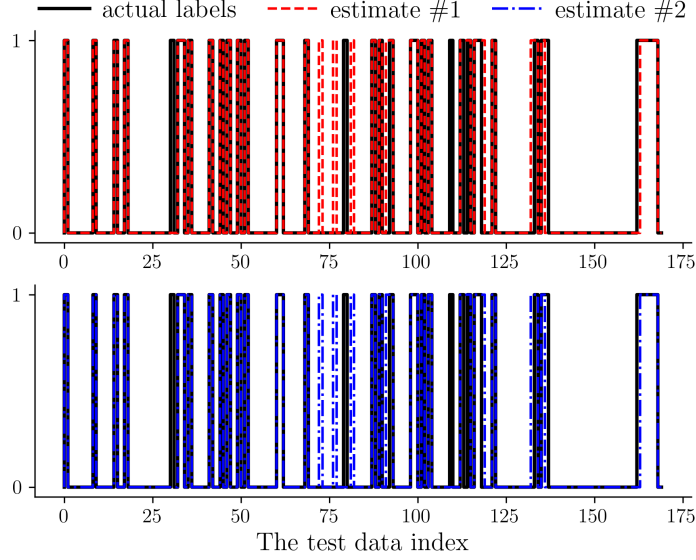


Figure 2: Comparison of the predicted labels with the actual labels for the test data of WDBC dataset with  $\beta = 0.05$ . Top: comparison of the labels for estimate #1. Bottom: the same for estimate #2.

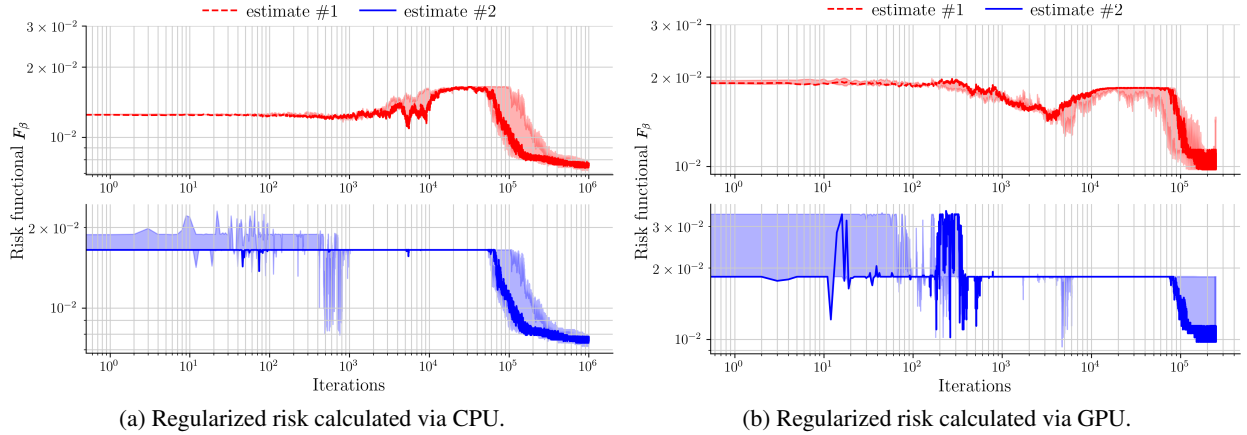


Figure 3: The solid line shows the regularized risk functional  $F_\beta$  versus the number of proximal recursions shown for the WDBC dataset with  $\beta = 0.05$ . The shadow shows the  $F_\beta$  variation range for different values of  $\beta \in \{0.03, 0.05, 0.07\}$ .

**Computational Complexity.** In this case study, we determine the computational complexity of PROXLEARN as follows. Letting

$$\begin{aligned} \mathbf{a}_{k-1} &:= (a_{k-1}^1 \ \dots \ a_{k-1}^N)^\top, \\ \mathbf{b}_{k-1} &= (b_{k-1}^1 \ \dots \ b_{k-1}^N)^\top, \\ \mathbf{W}_{k-1} &= (\mathbf{w}_{k-1}^1 \ \dots \ \mathbf{w}_{k-1}^N)^\top, \end{aligned}$$

we create the  $N \times n_{\text{data}}$  matrix

$$\mathbf{P}_{k-1} := (\mathbf{a}_{k-1} \mathbf{1}^\top) \odot \tanh(\mathbf{W}_{k-1} \mathbf{X}^\top + \mathbf{b}_{k-1} \mathbf{1}^\top), \quad (22)$$

which has complexity  $O(n_{\text{data}} N n_x)$ . The subsequent creation of matrix  $\mathbf{U}_{k-1}$  in line 3 of 2 has complexity  $O(n_{\text{data}} N^2)$ , and creating  $\mathbf{v}_{k-1}$  and  $\mathbf{u}_{k-1}$  takes complexity  $O(N n_{\text{data}})$  and  $O(N^2)$  respectively.



$\beta$	Estimate #1	Estimate #2	Runtime (hr)
0.03	91.18%	91.18%	1.415
0.05	91.18%	92.94%	1.533
0.07	90.59%	91.76%	1.704

Table 2: Classification accuracy after  $2.5 \times 10^5$  iterations, run on a Jetson TX2, with improvements to runtime.

We derive the relevant derivatives of  $\mathbf{v}_{k-1}$  and  $\mathbf{u}_{k-1}$  in the Supplementary Material. The complexity in calculating these derivatives is  $O(N^2 n_{\text{data}} n_x)$ . Updating  $\Theta_{k-1}$  using these results has complexity of  $O(Np) = O(Nn_x)$ . Therefore, the process of updating  $\Theta_{k-1}$  via EULERMARUYAMA is  $O(N^2 n_{\text{data}} n_x)$ .

The significant complexity in the remainder of PROXLEARN are the construction of matrix  $\mathbf{C}_k$  in line 3, and the matrix-vector multiplications within the while loop in lines 11 and 12.

The creation of the  $N \times N$  matrix  $\mathbf{C}_k$ , in which each element is the vector norm of a  $n_x \times 1$  vector, is  $O(n_x N^2)$ . In a worst-case scenario, the while loop runs  $L$  times. The operations of leading complexity within the while loop are the multiplications of the  $\Gamma_k$  matrix of size  $N \times N$  with the  $N \times 1$  vectors, which have a complexity of  $O(N^2)$ . Therefore, the while loop has a complexity of  $O(LN^2)$ .

Updating  $\varrho_{k-1}$  thus has a complexity of  $O((n_x + L)N^2)$ . In practice, the while loop typically ends far before reaching the maximum number of iterations  $L$ .

From this analysis, we find that the overall complexity of PROXLEARN is  $O(N^2(n_{\text{data}} n_x + L))$ .

## 5 CASE STUDY: MULTI-CLASS CLASSIFICATION

In the second case study, we apply the proposed algorithm to a ten-class classification problem using the Semeion Handwritten Digit (hereafter SHD) Data Set [19]. This numerical experiment is performed on the Jetson TX2 described above.

**SHD Data Set.** The SHD Data Set consists of 1593 handwritten digits. By viewing each digit as  $16 \times 16$  pixel image, each image is represented by  $n_x = 16^2 = 256$  features. Each feature is a boolean value indicating whether a particular pixel is filled. We subsequently re-scale these features such that  $\mathbf{x}_i \in \{-1, 1\}^{n_x}$ .

**Adaptations to PROXLEARN for Multi-Class Case.** To apply PROXLEARN for a multi-class case, we make several adaptations. For instance, rather than attempting to determine  $f(\mathbf{x}) \approx y$ , we redefine  $f(\mathbf{x})$  to represent a mapping of input data to the predicted likelihood of the correct label. We therefore redefine the variables, parameters, and risk function as follows.

Each label is represented by a  $1 \times 10$  vector of booleans, stored in a  $n_{\text{data}} \times 10$  matrix  $\mathbf{Y}$  where  $Y_{i,j} = 1$  if the  $i^{\text{th}}$  data point  $\mathbf{x}_i$  has label  $j$ , and  $Y_{i,j} = 0$  otherwise.

We construct the  $N \times n_{\text{data}}$  matrix  $\mathbf{P}_{k-1}$  by defining the  $(j, i)$  element of  $\mathbf{P}_{k-1}$  as

$$\mathbf{P}_{k-1}(j, i) := \Phi(\theta_{k-1}^j, \mathbf{X}(i, :), \mathbf{Y}(i, :)) := \left\langle \text{SOFTMAX}(\mathbf{X}(i, :)(\theta_{k-1}^j)^\top), (\mathbf{Y}(i, :))^\top \right\rangle \quad (23)$$

where  $\langle \cdot, \cdot \rangle$  denotes the standard Euclidean inner product. The SOFTMAX function in (23) produces a 10 by 1 vector of non-negative entries that sum to 1. By taking the inner product of this vector with the boolean vector  $\mathbf{Y}(i, :)$ , we define  $\mathbf{P}_{k-1}(j, i) = \Phi(\theta_{k-1}^j, \mathbf{X}(i, :), \mathbf{Y}(i, :))$  as the perceived likelihood that the data point  $i$  is labeled correctly by sample  $j$ . As our model improves, this value approaches 1, which also causes the probability of an incorrect label to drop.

As this newly defined  $\mathbf{P}_{k-1}$  does not call for bias or scaling, the weights alone are stored in the  $N \times p$  matrix  $\Theta_{k-1}$ . In this case,  $p := 10n_x$ , as each of the  $n_x$  features requires a distinct weight for each of the ten labels. For convenience, we reshape  $\Theta_{k-1} = (\theta_{k-1}^1, \dots, \theta_{k-1}^{10})$ , where each  $\theta_{k-1}^i$  is a  $10 \times n_x$  matrix. Therefore,  $\Theta_{k-1}$  is a  $10 \times n_x \times N$  tensor.

We set  $\varrho_0 \equiv \text{Unif}([-1, 1]^{n_x})$ , a uniform joint density function supported over  $n_x = 256$  dimensional mean field parameter space. We redefine the unregularized risk to reflect our new  $\Phi$  as follows:

$$F(\rho) := \mathbb{E}_{(\mathbf{x}, \mathbf{y})} \left( 1 - \int_{\mathbb{R}^p} \Phi(\mathbf{x}, \mathbf{y}, \boldsymbol{\theta}) \rho(\boldsymbol{\theta}) d\boldsymbol{\theta} \right)^2. \quad (24)$$

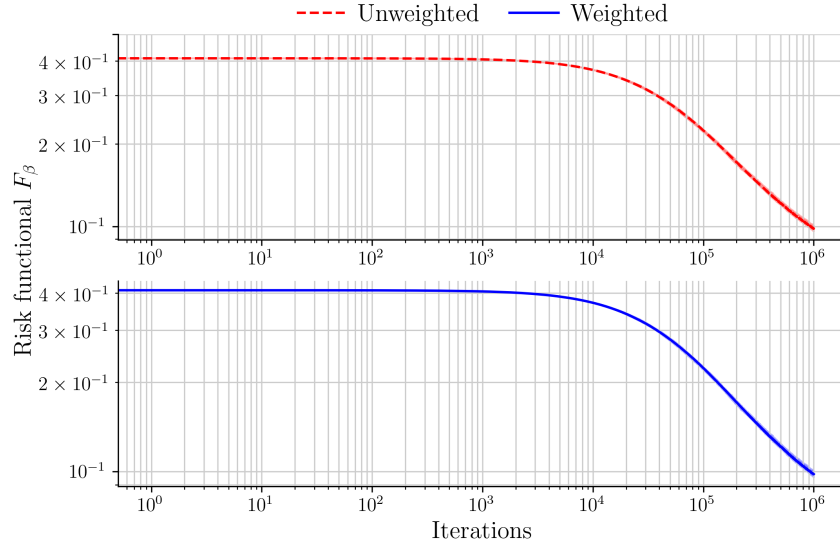


Figure 4: The solid line shows the average regularized risk functional  $F_\beta$  versus the number of proximal recursions shown for the Semeion dataset with  $\beta = 0.5$ . The narrow shadow shows the  $F_\beta$  variation range with the same  $\beta$  using the results of 30 independent runs, each starting from the same initial point cloud  $\{\theta_0^i, \varrho_0^i\}_{i=1}^N$ .

Expanding the above, we arrive at a form that resembles (9), now with the following adjusted definitions:

$$F_0 := 1, \quad (25)$$

$$V(\theta) := \mathbb{E}_{(x,y)}[-2\Phi(\theta, x, y)], \quad (26)$$

$$U(\theta, \tilde{\theta}) := \mathbb{E}_{(x,y)}[\Phi(\theta, x, y)\Phi(\tilde{\theta}, x, y)]. \quad (27)$$

We use the regularized risk functional  $F_\beta$  as in (13) where  $F$  now is given by (24). Due to the described changes in the structure of  $\Theta_{k-1}$ , the creation of  $C_k$  in line 3 of PROXLEARN results in a  $10 \times N \times N$  tensor, which we then sum along the ten element axis, returning an  $N \times N$  matrix.

Finally, we add a scaling in line 7 of EULERMARUYAMA, scaling the noise by a factor of  $1/100$ .

**Numerical Experiments.** With the adaptations mentioned above, we set the inverse temperature  $\beta = 0.5$ ,  $\epsilon = 10$ , the step size  $h = 10^{-3}$ , choose  $N = 100$  weighted uniform samples point cloud  $\{\theta_0^i, \varrho_0^i\}_{i=1}^N$  from  $\varrho_0 \equiv \text{Unif}([-1, 1]^{n_x})$  where the weights are the uniform PDF value at those samples. We take the first  $n_{\text{data}} = 1000$  images as training data, reserving the remaining  $n_{\text{test}} = 593$  images as test data, and execute 30 independent runs of our code, each for  $10^6$  proximal recursions.

To evaluate the training process, we create a matrix  $P_{k-1}^{\text{test}} \in \mathbb{R}^{N \times n_{\text{test}}}$ , using test data rather than training data, but otherwise defined as in (23). We then calculate a weighted approximation of  $F_\beta$ :

$$F_\beta \approx \frac{1}{n_{\text{test}}} \|\mathbf{1} - (P_{k-1}^{\text{test}})^\top \varrho\|_2^2, \quad (28)$$

and an unweighted approximation:

$$F_\beta \approx \frac{1}{n_{\text{test}}} \|\mathbf{1} - \frac{1}{N} (P_{k-1}^{\text{test}})^\top \mathbf{1}\|_2^2, \quad (29)$$

which we use to produce the risk and weighted risk log-log plots shown in Fig. 4.

Notably, despite the new activation function and the adaptations described above, our algorithm produces similar risk plots in the binary and multi-class cases. The run time for these  $10^6$  iterations is approximately 5.3 hours.

To evaluate our multi-class model, we calculate the percentage of accurately labeled test data by first taking ARGMAX  $(X_{\text{test}} \Theta_{k-1})$  along the ten-dimensional axis, to determine the predicted labels for each test data point using each

sample of  $\Theta_{k-1}$ . We then compare these predicted labels with the actual labels. We achieved slightly better than 61% accuracy of test data and 75% accuracy in training data.

**Updated Computational Complexity of PROXLEARN.** In the binary case, the creation of matrix  $C_k$  requires  $O(n_x N^2)$  flops. In the case of multi-class classification concerning  $m$  classes,  $C_k$  is redefined as the sum of  $m$  such matrices. Therefore, creating the updated matrix  $C_k$  takes  $O(mn_x N^2)$  flops. Thus, updating  $\varrho_{k-1}$  is of complexity  $O((mn_x + L)N^2)$ . The complexity of EULERMARUYAMA can be generalized from the discussion in Sec. 4.

## 6 CONCLUSIONS

This work presents a proximal mean field learning algorithm to train a shallow neural network in the over-parameterized regime. The proposed algorithm is meshless, non-parametric and implements the Wasserstein proximal recursions realizing the gradient descent of entropic-regularized risk. Two numerical case studies, one in binary and another in multi-class classification, demonstrate that the ideas of mean field learning can be attractive as computational framework, beyond its purely theoretical interests. Our contribution should be of interest to other learning and variational inference tasks such as the policy optimization, and adversarial learning. This work is expected to have no adverse societal impact.

## References

- [1] David Alvarez-Melis, Yair Schiff, and Youssef Mroueh. Optimizing functionals on the space of probabilities with input convex neural network. In *Annual Conference on Neural Information Processing Systems*, 2021.
- [2] Luigi Ambrosio, Nicola Gigli, and Giuseppe Savaré. *Gradient flows: in metric spaces and in the space of probability measures*. Springer Science & Business Media, 2005.
- [3] Brandon Amos, Lei Xu, and J Zico Kolter. Input convex neural networks. In *International Conference on Machine Learning*, pages 146–155. PMLR, 2017.
- [4] Andrew R Barron. Universal approximation bounds for superpositions of a sigmoidal function. *IEEE Transactions on Information theory*, 39(3):930–945, 1993.
- [5] Heinz H Bauschke, Patrick L Combettes, et al. *Convex analysis and monotone operator theory in Hilbert spaces*, volume 408. Springer, 2011.
- [6] Jean-David Benamou, Guillaume Carlier, and Maxime Laborde. An augmented Lagrangian approach to Wasserstein gradient flows and applications. *ESAIM: Proceedings and surveys*, 54:1–17, 2016.
- [7] Dimitri P Bertsekas et al. Incremental gradient, subgradient, and proximal methods for convex optimization: A survey. *Optimization for Machine Learning*, 2010(1-38):3, 2011.
- [8] Clément Bonet, Nicolas Courty, François Septier, and Lucas Drumetz. Sliced-Wasserstein gradient flows. *arXiv preprint arXiv:2110.10972*, 2021.
- [9] Clément Bonet, Nicolas Courty, François Septier, and Lucas Drumetz. Efficient gradient flows in sliced-wasserstein space. *arXiv preprint arxiv:2110.10972*, 2022.
- [10] Yann Brenier. Polar factorization and monotone rearrangement of vector-valued functions. *Communications on pure and applied mathematics*, 44(4):375–417, 1991.
- [11] Charlotte Bunne, Laetitia Papaxanthos, Andreas Krause, and Marco Cuturi. Proximal optimal transport modeling of population dynamics. In *International Conference on Artificial Intelligence and Statistics*, pages 6511–6528. PMLR, 2022.
- [12] Kenneth F Caluya and Abhishek Halder. Gradient flow algorithms for density propagation in stochastic systems. *IEEE Transactions on Automatic Control*, 65(10):3991–4004, 2019.
- [13] Guillaume Carlier, Vincent Duval, Gabriel Peyré, and Bernhard Schmitzer. Convergence of entropic schemes for optimal transport and gradient flows. *SIAM Journal on Mathematical Analysis*, 49(2):1385–1418, 2017.
- [14] José A Carrillo, Katy Craig, Li Wang, and Chaozhen Wei. Primal dual methods for Wasserstein gradient flows. *Foundations of Computational Mathematics*, 22(2):389–443, 2022.
- [15] Lenaic Chizat and Francis Bach. On the global convergence of gradient descent for over-parameterized models using optimal transport. *Advances in neural information processing systems*, 31, 2018.
- [16] Casey Chu, Jose Blanchet, and Peter Glynn. Probability functional descent: A unifying perspective on GANS, variational inference, and reinforcement learning. In *International Conference on Machine Learning*, pages 1213–1222. PMLR, 2019.

- [17] George Cybenko. Approximation by superpositions of a sigmoidal function. *Mathematics of control, signals and systems*, 2(4):303–314, 1989.
- [18] Carles Domingo-Enrich, Samy Jelassi, Arthur Mensch, Grant Rotskoff, and Joan Bruna. A mean-field analysis of two-player zero-sum games. *Advances in neural information processing systems*, 33:20215–20226, 2020.
- [19] Dheeru Dua and Casey Graff. UCI machine learning machine learning repository. 2017.
- [20] Charlie Frogner and Tomaso Poggio. Approximate inference with Wasserstein gradient flows. In *International Conference on Artificial Intelligence and Statistics*, pages 2581–2590. PMLR, 2020.
- [21] Abhishek Halder, Kenneth F Caluya, Bertrand Travacca, and Scott J Moura. Hopfield neural network flow: A geometric viewpoint. *IEEE Transactions on Neural Networks and Learning Systems*, 31(11):4869–4880, 2020.
- [22] Richard Jordan, David Kinderlehrer, and Felix Otto. The variational formulation of the Fokker–Planck equation. *SIAM journal on mathematical analysis*, 29(1):1–17, 1998.
- [23] Johan Karlsson and Axel Ringh. Generalized Sinkhorn iterations for regularizing inverse problems using optimal mass transport. *SIAM Journal on Imaging Sciences*, 10(4):1935–1962, 2017.
- [24] Diederik P Kingma and Jimmy Ba. Adam: A method for stochastic optimization. *arXiv preprint arXiv:1412.6980*, 2014.
- [25] Maxime Laborde. On some nonlinear evolution systems which are perturbations of Wasserstein gradient flows. *Topological Optimization and Optimal Transport: In the Applied Sciences*, 17:304–332, 2017.
- [26] Chang Liu, Jingwei Zhuo, Pengyu Cheng, Ruiyi Zhang, and Jun Zhu. Understanding and accelerating particle-based variational inference. In *International Conference on Machine Learning*, pages 4082–4092. PMLR, 2019.
- [27] Song Mei, Andrea Montanari, and Phan-Minh Nguyen. A mean field view of the landscape of two-layer neural networks. *Proceedings of the National Academy of Sciences*, 115(33):E7665–E7671, 2018.
- [28] Petr Mokrov, Alexander Korotin, Lingxiao Li, Aude Genevay, Justin M Solomon, and Evgeny Burnaev. Large-scale Wasserstein gradient flows. *Advances in Neural Information Processing Systems*, 34:15243–15256, 2021.
- [29] Youssef Mroueh and Truyen Nguyen. On the convergence of gradient descent in GANs: MMD GAN as a gradient flow. In *International Conference on Artificial Intelligence and Statistics*, pages 1720–1728. PMLR, 2021.
- [30] Neal Parikh, Stephen Boyd, et al. Proximal algorithms. *Foundations and trends® in Optimization*, 1(3):127–239, 2014.
- [31] Adam Paszke, Sam Gross, Soumith Chintala, Gregory Chanan, Edward Yang, Zachary DeVito, Zeming Lin, Alban Desmaison, Luca Antiga, and Adam Lerer. Automatic differentiation in pytorch. 2017.
- [32] Gabriel Peyré. Entropic approximation of Wasserstein gradient flows. *SIAM Journal on Imaging Sciences*, 8(4):2323–2351, 2015.
- [33] Julien Rabin, Gabriel Peyré, Julie Delon, and Marc Bernot. Wasserstein barycenter and its application to texture mixing. In *International Conference on Scale Space and Variational Methods in Computer Vision*, pages 435–446. Springer, 2011.
- [34] R Tyrrell Rockafellar. Augmented Lagrangians and applications of the proximal point algorithm in convex programming. *Mathematics of operations research*, 1(2):97–116, 1976.
- [35] R Tyrrell Rockafellar. Monotone operators and the proximal point algorithm. *SIAM journal on control and optimization*, 14(5):877–898, 1976.
- [36] Grant M Rotskoff and Eric Vanden-Eijnden. Neural networks as interacting particle systems: Asymptotic convexity of the loss landscape and universal scaling of the approximation error. *stat*, 1050:22, 2018.
- [37] Adil Salim, Anna Korba, and Giulia Luise. The Wasserstein proximal gradient algorithm. *Advances in Neural Information Processing Systems*, 33:12356–12366, 2020.
- [38] Filippo Santambrogio. {Euclidean, metric, and Wasserstein} gradient flows: an overview. *Bulletin of Mathematical Sciences*, 7(1):87–154, 2017.
- [39] Justin Sirignano and Konstantinos Spiliopoulos. Mean field analysis of neural networks: A central limit theorem. *Stochastic Processes and their Applications*, 130(3):1820–1852, 2020.
- [40] Marc Teboulle. Entropic proximal mappings with applications to nonlinear programming. *Mathematics of Operations Research*, 17(3):670–690, 1992.
- [41] Anthony C Thompson. On certain contraction mappings in a partially ordered vector space. *Proceedings of the American Mathematical Society*, 14(3):438–443, 1963.

- [42] Cédric Villani. *Optimal transport: old and new*, volume 338. Springer, 2009.
- [43] Cédric Villani. *Topics in optimal transportation*, volume 58. American Mathematical Soc., 2021.
- [44] Sofia Visa, Brian Ramsay, Anca L Ralescu, and Esther Van Der Knaap. Confusion matrix-based feature selection. *MAICS*, 710:120–127, 2011.
- [45] Junyu Zhang, Alec Koppel, Amrit Singh Bedi, Csaba Szepesvari, and Mengdi Wang. Variational policy gradient method for reinforcement learning with general utilities. *Advances in Neural Information Processing Systems*, 33:4572–4583, 2020.
- [46] Ruiyi Zhang, Changyou Chen, Chunyuan Li, and Lawrence Carin. Policy optimization as Wasserstein gradient flows. In *International Conference on Machine Learning*, pages 5737–5746. PMLR, 2018.

## A. Derivation of PROXLERN and its convergence

To derive the recursion given in PROXLERN, we first write the discrete version of (17) as follows

$$\mathbf{q}_k = \arg \min_{\mathbf{q}} \left\{ \min_{\mathbf{M} \in \Pi(\mathbf{q}_{k-1}, \mathbf{q})} \frac{1}{2} \langle \mathbf{C}_k, \mathbf{M} \rangle + h \langle \mathbf{v}_{k-1} + \mathbf{U}_{k-1} \mathbf{q}_{k-1} + \beta^{-1} \log \mathbf{q}, \mathbf{q} \rangle \right\}, \quad k \in \mathbb{N}, \quad (30)$$

where

$$\Pi(\mathbf{q}_{k-1}, \mathbf{q}) := \{\mathbf{M} \in \mathbb{R}^{N \times N} \mid \mathbf{M} \geq \mathbf{0} \text{ (elementwise)}, \mathbf{M}\mathbf{1} = \mathbf{q}_{k-1}, \mathbf{M}^\top \mathbf{1} = \mathbf{q}\}, \quad (31a)$$

$$\mathbf{v}_{k-1} \equiv V(\boldsymbol{\theta}_{k-1}), \quad (31b)$$

$$\mathbf{U}_{k-1} \equiv U(\boldsymbol{\theta}_{k-1}, \tilde{\boldsymbol{\theta}}_{k-1}), \quad (31c)$$

and  $\mathbf{C}_k \in \mathbb{R}^{N \times N}$  denotes the squared Euclidean distance matrix such that  $\mathbf{C}_k(i, j) := \|\boldsymbol{\theta}_k^i - \boldsymbol{\theta}_{k-1}^j\|_2^2$  for all  $i, j \in [N]$ . Then, we follow a “regularize-then-dualize” approach.

In particular, we regularize (30) by adding the entropic regularization  $H(\mathbf{M}) := \langle \mathbf{M}, \log \mathbf{M} \rangle$ , and write

$$\mathbf{q}_k = \arg \min_{\mathbf{q}} \left\{ \min_{\mathbf{M} \in \Pi(\mathbf{q}_{k-1}, \mathbf{q})} \frac{1}{2} \langle \mathbf{C}_k, \mathbf{M} \rangle + \epsilon H(\mathbf{M}) + h \langle \mathbf{v}_{k-1} + \mathbf{U}_{k-1} \mathbf{q}_{k-1} + \beta^{-1} \log \mathbf{q}, \mathbf{q} \rangle \right\}, \quad k \in \mathbb{N} \quad (32)$$

where  $\epsilon > 0$  is a regularization parameter.

Following [23, Lemma 3.5], [12, Sec. III], the Lagrange dual problem associated with (32) is

$$(\boldsymbol{\lambda}_0^{\text{opt}}, \boldsymbol{\lambda}_1^{\text{opt}}) = \arg \max_{\boldsymbol{\lambda}_0, \boldsymbol{\lambda}_1 \in \mathbb{R}^N} \left\{ \langle \boldsymbol{\lambda}_0, \mathbf{q}_{k-1} \rangle - \hat{F}_\beta^*(-\boldsymbol{\lambda}_1) - \frac{\epsilon}{h} \left( \exp(\boldsymbol{\lambda}_0^\top h/\epsilon) \exp(-\mathbf{C}_k/2\epsilon) \exp(\boldsymbol{\lambda}_1 h/\epsilon) \right) \right\} \quad (33)$$

where

$$\hat{F}_\beta^*(\cdot) := \sup_{\vartheta} \{ \langle \cdot, \vartheta \rangle - \hat{F}_\beta(\vartheta) \} \quad (34)$$

is the Legendre-Fenchel conjugate of the free energy  $\hat{F}_\beta$  in (17), and the optimal coupling matrix  $\mathbf{M}^{\text{opt}} := [m^{\text{opt}}(i, j)]_{i, j=1}^N$  in (32) has the Sinkhorn form

$$m^{\text{opt}}(i, j) = \exp(\boldsymbol{\lambda}_0(i)h/\epsilon) \exp(-\mathbf{C}_k(i, j)/(2\epsilon)) \exp(\boldsymbol{\lambda}_1(j)h/\epsilon). \quad (35)$$

To solve (33), considering (13), we write the “discrete free energy” as

$$\hat{F}_\beta(\mathbf{q}) = \langle \mathbf{v}_{k-1} + \mathbf{U}_{k-1} \mathbf{q}_{k-1} + \beta^{-1} \log \mathbf{q}, \mathbf{q} \rangle. \quad (36)$$

Its Legendre-Fenchel conjugate, by (34), is given by

$$\hat{F}_\beta^*(\boldsymbol{\lambda}) := \sup_{\mathbf{q}} \{ \boldsymbol{\lambda}^\top \mathbf{q} - \mathbf{v}_{k-1}^\top \mathbf{q} - \mathbf{q}^\top \mathbf{U}_{k-1} \mathbf{q}_{k-1} - \beta^{-1} \mathbf{q}^\top \log \mathbf{q} \}. \quad (37)$$

Setting the gradient of the objective function in (37) w.r.t.  $\mathbf{q}$  to zero, and solving for  $\mathbf{q}$  yields

$$\mathbf{q}_{\max} = \exp(\beta(\boldsymbol{\lambda} - \mathbf{v}_{k-1} - \beta^{-1} \mathbf{1} - \mathbf{U}_{k-1} \mathbf{q}_{k-1})). \quad (38)$$

Substituting (38) back into (37), we obtain

$$\hat{F}_\beta^*(\boldsymbol{\lambda}) = \beta^{-1} \mathbf{1} \exp(\beta(\boldsymbol{\lambda} - \mathbf{v}_{k-1} - \mathbf{U}_{k-1} \mathbf{q}_{k-1}) - \mathbf{1}). \quad (39)$$

Fixing  $\boldsymbol{\lambda}_0$ , and taking the gradient of the objective in (33) w.r.t.  $\boldsymbol{\lambda}_1$  gives

$$\exp(\boldsymbol{\lambda}_1 h/\epsilon) \odot \left( \exp(-\mathbf{C}_k/2\epsilon)^\top \exp(\boldsymbol{\lambda}_0 h/\epsilon) \right) = \exp(-\beta \mathbf{v}_{k-1} - \beta \mathbf{U}_{k-1} \mathbf{q}_{k-1} - \mathbf{1}) \odot (\exp(\boldsymbol{\lambda}_1 h/\epsilon))^{-\frac{\beta \epsilon}{h}}. \quad (40)$$

Likewise, fixing  $\boldsymbol{\lambda}_1$ , and taking the gradient of the objective in (33) w.r.t.  $\boldsymbol{\lambda}_0$ , gives

$$\exp(\boldsymbol{\lambda}_0 h/\epsilon) \odot (\exp(-\mathbf{C}_k/2\epsilon) \exp(\boldsymbol{\lambda}_1 h/\epsilon)) = \mathbf{q}_{k-1}. \quad (41)$$

Next, letting  $\Gamma_k := \exp(-C_k/2\epsilon)$ ,  $\mathbf{q} := \exp(\lambda_0 h/\epsilon)$ ,  $\mathbf{z} := \exp(\lambda_1 h/\epsilon)$ , and  $\xi_{k-1} := \exp(-\beta \mathbf{v}_{k-1} - \beta \mathbf{U}_{k-1} \varrho_{k-1} - 1)$ , we write (40) as

$$\mathbf{z} \odot (\Gamma_k^\top \mathbf{q}) = \xi_{k-1} \odot \mathbf{z}^{-\frac{\beta\epsilon}{h}}, \quad (42)$$

and (41) as

$$\mathbf{q} \odot (\Gamma_k \mathbf{z}) = \varrho_{k-1}. \quad (43)$$

Using (31a), we then have

$$\varrho_k = (\mathbf{M}^{\text{opt}})^\top \mathbf{1} = \sum_{j=1}^N m^{\text{opt}}(j, i) = \mathbf{z}(i) \sum_{j=1}^N \Gamma_k(j, i) \mathbf{q}(j) = \mathbf{z} \odot \Gamma_k^\top \mathbf{q}. \quad (44)$$

**Remark 1.** Note that in Algorithm 1 (i.e., PROXLEARN) presented in Sec. 3, the lines 11, 12, and 19 correspond to (42), (43), and (44), respectively.

**Proposition 1.** The recursions given in lines 7–18 in Algorithm 1 PROXLEARN converges to unique fixed point  $(\mathbf{q}^{\text{opt}}, \mathbf{z}^{\text{opt}}) \in \mathbb{R}_{>0}^N \times \mathbb{R}_{>0}^N$ . Consequently, the proximal update (44) (i.e., line 19 in Algorithm 1) is unique.

*Proof.* Notice that the mappings  $(\mathbf{q}(\cdot, \ell), \mathbf{z}(\cdot, \ell)) \mapsto (\mathbf{q}(\cdot, \ell+1), \mathbf{z}(\cdot, \ell+1))$  given in line 11 and 12 in Algorithm 1, are cone preserving since the mapping preserves the product orthant  $\mathbb{R}_{>0}^N \times \mathbb{R}_{>0}^N$ . This is a direct consequence of the definition of  $\mathbf{q}, \mathbf{z}$  in terms of  $\lambda_0, \lambda_1$ .

Now the idea is to show that the recursions in line 11 and 12 in Algorithm 1, as composite nonlinear maps, are in fact contractive w.r.t. a suitable metric on this cone. Following [12, Theorem 3], the  $\mathbf{z}$  iteration given in line 11 in Algorithm 1, PROXLEARN, for  $\ell = 1, 2, \dots$ , is strictly contractive in the Thompson's part metric [41] and thanks to the contraction mapping theorem, converges to a unique fixed point  $\mathbf{z}^{\text{opt}} \in \mathbb{R}_{>0}^N$ . Note that our definition of  $\xi_{k-1}$  is slightly different compared to the same in [12, Theorem 3], but this does not affect the proof. From definition of  $C_k$ , we have  $C_k \in [0, \infty)$  which implies  $\Gamma_k(i, j) \in (0, 1]$ ; therefore,  $\Gamma_k$  is a positive linear map for each  $k \in \mathbb{N}$ . Thus, by (linear) Perron-Frobenius theorem, the linear maps  $\Gamma_k$  are contractive. Consequently the  $\mathbf{q}$  iterates also converge to unique fixed point  $\mathbf{q}^{\text{opt}} \in \mathbb{R}_{>0}^N$ .

Since converged pair  $(\mathbf{q}^{\text{opt}}, \mathbf{z}^{\text{opt}}) \in \mathbb{R}_{>0}^N \times \mathbb{R}_{>0}^N$  is unique, so is the proximal update (44), i.e., line 19 in Algorithm 1.  $\blacksquare$

## B. Proof of Theorem 1

Our proof follows the general development in [25, Sec. 12.3]. In the following, we sketch the main ideas.

We have the semi-implicit free energy

$$\hat{F}_\beta(\varrho, \varrho_{k-1}) = \underbrace{\mathbb{E}_\varrho \left[ F_0 + V(\boldsymbol{\theta}) + \int_{\mathbb{R}^p} U(\boldsymbol{\theta}, \tilde{\boldsymbol{\theta}}) \varrho_{k-1}(\tilde{\boldsymbol{\theta}}) d\tilde{\boldsymbol{\theta}} \right]}_{=: \mathcal{V}_{\text{advec}}(\varrho)} + \beta^{-1} \mathbb{E}_\varrho [\log \varrho], \quad k \in \mathbb{N},$$

wherein the summand  $\mathcal{V}_{\text{advec}}(\varrho) := \mathbb{E}_\varrho \left[ F_0 + V(\boldsymbol{\theta}) + \int_{\mathbb{R}^p} U(\boldsymbol{\theta}, \tilde{\boldsymbol{\theta}}) \varrho_{k-1}(\tilde{\boldsymbol{\theta}}) d\tilde{\boldsymbol{\theta}} \right]$  is linear in  $\varrho$ , and contributes as an effective advection potential energy. The remaining summand  $\beta^{-1} \mathbb{E}_\varrho [\log \varrho]$  results in from diffusion regularization and contributes as an internal energy term.

We note from (10) that the functional  $\mathcal{V}_{\text{advec}}(\varrho)$  is lower bounded for all  $\varrho \in \mathcal{P}_2(\mathbb{R}^p)$ . Furthermore,  $\mathcal{V}_{\text{advec}}(\varrho)$  and  $\nabla \mathcal{V}_{\text{advec}}(\varrho)$  are uniformly Lipschitz continuous, i.e., there exists  $C_1 > 0$  such that

$$\|\nabla \mathcal{V}_{\text{advec}}(\varrho)\|_{L^\infty(\mathbb{R}^p)} + \|\nabla^2 \mathcal{V}_{\text{advec}}(\varrho)\|_{L^\infty(\mathbb{R}^p)} \leq C_1 \quad \forall \varrho \in \mathcal{P}_2(\mathbb{R}^p),$$

where the constant  $C_1 > 0$  is independent of  $\varrho$ , and  $\nabla^2$  denotes the Euclidean Hessian operator. Moreover, there exists  $C_2 > 0$  such that for all  $\varrho, \tilde{\varrho} \in \mathcal{P}_2(\mathbb{R}^p)$ , we have

$$\|\nabla \mathcal{V}_{\text{advec}}(\varrho) - \nabla \mathcal{V}_{\text{advec}}(\tilde{\varrho})\|_{L^\infty(\mathbb{R}^p)} \leq C_2 W_2(\varrho, \tilde{\varrho}).$$

Thus,  $\mathcal{V}_{\text{advec}}(\varrho)$  satisfy the hypotheses in [25, Sec. 12.2].

For  $t \in [0, T]$ , we say that  $\rho(t, \boldsymbol{\theta}) \in C([0, T], \mathcal{P}_2(\mathbb{R}^p))$  is a weak solution of the IVP (15) if for any smooth compactly supported test function  $\varphi \in C_c^\infty([0, \infty) \times \mathbb{R}^p)$ , we have

$$\int_0^\infty \int_{\mathbb{R}^p} \left( \left( \frac{\partial \varphi}{\partial t} - \langle \nabla \varphi, \nabla \mathcal{V}_{\text{advec}}(\varrho) \rangle \right) \rho + \beta^{-1} \rho \Delta \varphi \right) d\boldsymbol{\theta} dt = - \int_{\mathbb{R}^p} \varphi(t=0, \boldsymbol{\theta}) \rho_0(\boldsymbol{\theta}). \quad (45)$$

Following [25, Sec. 12.2], under the stated hypotheses on  $\mathcal{V}_{\text{advec}}(\varrho)$ , there exists weak solution of the IVP (15) that is continuous w.r.t. the  $W_2$  metric.

The remaining of the proof follows the outline below.

- Using the Dunford-Pettis' theorem, establish that the sequence of functions  $\{\varrho_k(h, \boldsymbol{\theta})\}_{k \in \mathbb{N}}$  solving (17) is unique.
- Define the interpolation  $\varrho_h(t) := \varrho_k(h, \boldsymbol{\theta})$  if  $t \in ((k-1)h, kh]$  for all  $k \in \mathbb{N}$ . Then establish that  $\varrho_h(t)$  solves a discrete approximation of (45).
- Finally combine the gradient estimates and pass to the limit  $h \downarrow 0$ , to conclude that  $\rho_h(t)$  in this limit solves converges to the weak solution of (45) in strong  $L^1(\mathbb{R}^p)$  sense.

For the detailed calculations on the passage to the limit, we refer the readers to [25, Sec. 12.5]. ■

### C. Expressions involving derivatives of $\mathbf{v}$

We define matrices

$$\begin{aligned} \mathbf{T} &:= \tanh(\mathbf{W}\mathbf{X}^\top + \mathbf{b}\mathbf{1}^\top), \\ \mathbf{S} &:= \text{sech}^2(\mathbf{W}\mathbf{X}^\top + \mathbf{b}\mathbf{1}^\top), \end{aligned}$$

where  $\mathbf{1}$  is a vector of all ones of size  $n_{\text{data}} \times 1$ , and the functions  $\tanh(\cdot)$  and  $\text{sech}^2(\cdot)$  are elementwise. Notice that  $\mathbf{T}, \mathbf{S} \in \mathbb{R}^{N \times n_{\text{data}}}$ . Then

$$\mathbf{v} = -\frac{2}{n_{\text{data}}} \mathbf{a} \odot (\tanh(\mathbf{W}\mathbf{X}^\top + \mathbf{b}\mathbf{1}^\top) \mathbf{y}) = -\frac{2}{n_{\text{data}}} \mathbf{a} \odot (\mathbf{T} \mathbf{y}).$$

**Proposition 2.** *With the above notations in place, we have*

$$\frac{\partial \mathbf{v}}{\partial \mathbf{a}} \mathbf{1} = \sum_{k=1}^N \frac{\partial \mathbf{v}_k}{\partial \mathbf{a}} = -\frac{2}{n_{\text{data}}} \mathbf{T} \mathbf{y}, \quad (46)$$

and

$$\frac{\partial \mathbf{v}}{\partial \mathbf{b}} \mathbf{1} = \sum_{k=1}^N \frac{\partial \mathbf{v}_k}{\partial \mathbf{b}} = -\frac{2}{n_{\text{data}}} \mathbf{a} \odot \mathbf{S} \mathbf{y}. \quad (47)$$

Furthermore,

$$\sum_{k=1}^N \frac{\partial \mathbf{v}_k}{\partial \mathbf{W}} = -\frac{2}{n_{\text{data}}} [(\mathbf{a}\mathbf{1}^\top) \odot (\mathbf{S}(\mathbf{X} \odot \mathbf{y}\mathbf{1}^\top))]. \quad (48)$$

*Proof.* The  $k^{\text{th}}$  element of  $\mathbf{v}$  is  $\mathbf{v}_k = -\frac{2}{n_{\text{data}}} \mathbf{a}_k \sum_{i=1}^{n_{\text{data}}} [\mathbf{T}_{k,i} \mathbf{y}_i]$ . Thus,

$$\frac{\partial \mathbf{v}_k}{\partial \mathbf{a}_j} = \begin{cases} 0 & \text{for } k \neq j, \\ -\frac{2}{n_{\text{data}}} \sum_{i=1}^{n_{\text{data}}} [\mathbf{T}_{k,i} \mathbf{y}_i] & \text{for } k = j. \end{cases}$$

So the matrix  $\frac{\partial \mathbf{v}}{\partial \mathbf{a}}$  is diagonal, and  $[\frac{\partial \mathbf{v}}{\partial \mathbf{a}} \mathbf{1}]_k = -\frac{2}{n_{\text{data}}} \sum_{i=1}^{n_{\text{data}}} [\mathbf{T}_{k,i} \mathbf{y}_i] = -\frac{2}{n_{\text{data}}} [\mathbf{T} \mathbf{y}]_k$ . Hence, we obtain

$$\frac{\partial \mathbf{v}}{\partial \mathbf{a}} \mathbf{1} = -\frac{2}{n_{\text{data}}} \mathbf{T} \mathbf{y},$$

which is (46).



On the other hand,

$$\frac{\partial v_k}{\partial b_k} = \frac{\partial}{\partial b_k} \left[ -\frac{2}{n_{\text{data}}} \mathbf{a}_k \sum_{i=1}^{n_{\text{data}}} [\mathbf{T}_{k,i} \mathbf{y}_i] \right] = -\frac{2}{n_{\text{data}}} \mathbf{a}_k \sum_{i=1}^{n_{\text{data}}} \frac{\partial}{\partial b_k} [\mathbf{T}_{k,i} \mathbf{y}_i].$$

Note that

$$\frac{\partial}{\partial b_k} [\mathbf{T}_{k,i} \mathbf{y}_i] = \frac{\partial}{\partial b_k} \tanh \left( \sum_{j=1}^{n_x} (\mathbf{W}_{k,j} \mathbf{X}_{i,j}) + b_k \right) \mathbf{y}_i = \text{sech}^2 \left( \sum_{j=1}^{n_x} (\mathbf{W}_{k,j} \mathbf{X}_{i,j}) + b_k \right) \mathbf{y}_i = \mathbf{S}_{k,i} \mathbf{y}_i.$$

Therefore,

$$\frac{\partial v_k}{\partial b_j} = \begin{cases} 0 & \text{for } k \neq j, \\ -\frac{2}{n_{\text{data}}} \mathbf{a}_k \sum_{i=1}^{n_{\text{data}}} [\mathbf{S}_{k,i} \mathbf{y}_i] & \text{for } k = j. \end{cases}$$

As the matrix  $\frac{\partial \mathbf{v}}{\partial \mathbf{b}}$  is diagonal, we get

$$\left[ \frac{\partial \mathbf{v}}{\partial \mathbf{b}} \mathbf{1} \right]_k = -\frac{2}{n_{\text{data}}} \mathbf{a}_k \sum_{i=1}^{n_{\text{data}}} [\mathbf{S}_{k,i} \mathbf{y}_i] = -\frac{2}{n_{\text{data}}} \mathbf{a}_k [\mathbf{S} \mathbf{y}]_k,$$

and so

$$\frac{\partial \mathbf{v}}{\partial \mathbf{b}} \mathbf{1} = -\frac{2}{n_{\text{data}}} \mathbf{a} \odot \mathbf{S} \mathbf{y},$$

which is indeed (47).

Likewise, we take an element-wise approach to the derivatives with respect to weights  $\mathbf{W}_{k,m}$ . Note that such a weight  $\mathbf{W}_{k,m}$  will only appear in the  $k$ th element of  $\mathbf{v}$ , and so we only need to compute

$$\frac{\partial v_k}{\partial \mathbf{W}_{k,m}} = -\frac{2}{n_{\text{data}}} \mathbf{a}_k \sum_{i=1}^{n_{\text{data}}} \frac{\partial}{\partial \mathbf{W}_{k,m}} [\mathbf{T}_{k,i} \mathbf{y}_i].$$

Since

$$\frac{\partial}{\partial \mathbf{W}_{k,m}} [\mathbf{T}_{k,i} \mathbf{y}_i] = \frac{\partial}{\partial \mathbf{W}_{k,m}} \tanh \left( \sum_{j=1}^{n_x} (\mathbf{W}_{k,j} \mathbf{X}_{i,j}) + b_k \right) \mathbf{y}_i = \text{sech}^2 \left( \sum_{j=1}^{n_x} (\mathbf{W}_{k,j} \mathbf{X}_{i,j}) + b_k \right) \mathbf{X}_{i,m} \mathbf{y}_i = \mathbf{S}_{k,i} \mathbf{X}_{i,m} \mathbf{y}_i,$$

we have

$$\frac{\partial v_k}{\partial \mathbf{W}_{m,j}} = \begin{cases} 0 & \text{for } k \neq m, \\ -\frac{2}{n_{\text{data}}} \mathbf{a}_k \sum_{i=1}^{n_{\text{data}}} [\mathbf{S}_{k,i} \mathbf{X}_{i,m} \mathbf{y}_i] & \text{for } k = m. \end{cases}$$

Thus,

$$\sum_{k=1}^N \frac{\partial v_k}{\partial \mathbf{W}_{m,j}} = -\frac{2}{n_{\text{data}}} \mathbf{a}_m \sum_{i=1}^{n_{\text{data}}} [\mathbf{S}_{m,i} \mathbf{X}_{i,m} \mathbf{y}_i] = -\frac{2}{n_{\text{data}}} \mathbf{a}_m [\mathbf{S} (\mathbf{X} \odot (\mathbf{y} \mathbf{1}^\top))]_{m,j}.$$

Therefore, considering  $\mathbf{1} \in \mathbb{R}^{n_x}$ , we write

$$\sum_{k=1}^N \frac{\partial v_k}{\partial \mathbf{W}} = -\frac{2}{n_{\text{data}}} [(\mathbf{a} \mathbf{1}^\top) \odot (\mathbf{S} (\mathbf{X} \odot \mathbf{y} \mathbf{1}^\top))],$$

thus arriving at (48). This completes the proof.  $\blacksquare$

## D. Expressions involving derivatives of $\mathbf{u}$

Expressions involving the derivatives of  $\mathbf{u}$ , are summarized in the Proposition next. These results find use in Sec. 4. We start by noting that

$$\mathbf{u} = \frac{1}{n_{\text{data}}} (\mathbf{1}^\top \mathbf{a} \odot \mathbf{T}) (\mathbf{1}^\top \mathbf{a} \odot \mathbf{T})^\top \boldsymbol{\rho} = \frac{1}{n_{\text{data}}} (\mathbf{1}^\top \mathbf{a} \odot \mathbf{T}) (\mathbf{a}^\top \mathbf{1} \odot \mathbf{T}^\top) \boldsymbol{\rho}.$$

**Proposition 3.** *With the above notations in place, we have*

$$\underbrace{\frac{\partial \mathbf{u}}{\partial \mathbf{a}}}_{N \times N} \underbrace{\mathbf{1}}_{N \times 1} = \frac{1}{n_{\text{data}}} \left[ ((\varrho \mathbf{a}^\top) \odot (\mathbf{T} \mathbf{T}^\top)) \mathbf{1} + \mathbf{1} (\mathbf{a} \odot \varrho)^\top \mathbf{T} \mathbf{T}^\top \mathbf{1} \right], \quad (49)$$

and

$$\underbrace{\frac{\partial \mathbf{u}}{\partial \mathbf{b}}}_{N \times N} \underbrace{\mathbf{1}}_{N \times 1} = \frac{1}{n_{\text{data}}} \left[ ((\mathbf{a} \mathbf{1}^\top) \odot (\mathbf{S} \mathbf{T}^\top) \odot (\mathbf{1} (\mathbf{a} \odot \varrho)^\top)) \mathbf{1} + ((\mathbf{1} \mathbf{a}^\top) \odot (\mathbf{S} \mathbf{T}^\top) \odot ((\mathbf{a} \odot \varrho) \mathbf{1}^\top)) \mathbf{1} \right]. \quad (50)$$

Furthermore,

$$\sum_{k=1}^N \frac{\partial \mathbf{u}}{\partial \mathbf{W}_{i,j}} = \frac{1}{n_{\text{data}}} \sum_{k=1}^N \sum_{m=1}^{n_{\text{data}}} a_i a_k (\varrho_i + \varrho_k) T_{k,m} S_{i,m} X_{m,j}. \quad (51)$$

*Proof.* Letting  $\mathbf{t}_i^\top$  denote the  $i$ th row of  $\mathbf{T}$ , we rewrite  $\mathbf{u}$  as follows:

$$\mathbf{u} = \frac{1}{n_{\text{data}}} \begin{bmatrix} a_1 \mathbf{t}_1^\top \\ \vdots \\ a_N \mathbf{t}_N^\top \end{bmatrix} [\rho_1 a_1 \mathbf{t}_1 + \dots + \rho_N a_N \mathbf{t}_N] = \frac{1}{n_{\text{data}}} \begin{bmatrix} a_1 \mathbf{t}_1^\top (\rho_1 a_1 \mathbf{t}_1 + \dots + \rho_N a_N \mathbf{t}_N) \\ \vdots \\ a_N \mathbf{t}_N^\top (\rho_1 a_1 \mathbf{t}_1 + \dots + \rho_N a_N \mathbf{t}_N) \end{bmatrix}.$$

For  $i \neq k$ , we thus have

$$\frac{\partial u_i}{\partial a_k} = \frac{1}{n_{\text{data}}} a_i \mathbf{t}_i^\top (\rho_k \mathbf{t}_k) = \frac{1}{n_{\text{data}}} a_i \rho_k \mathbf{t}_i^\top \mathbf{t}_k.$$

Likewise, for  $i = k$ , we have

$$\frac{\partial u_k}{\partial a_k} = \frac{1}{n_{\text{data}}} a_k \rho_k \mathbf{t}_k^\top \mathbf{t}_k + \frac{1}{n_{\text{data}}} \mathbf{t}_k^\top (\rho_1 a_1 \mathbf{t}_1 + \dots + \rho_N a_N \mathbf{t}_N).$$

Combining the above, we obtain  $\frac{\partial \mathbf{u}}{\partial \mathbf{a}}$ , and hence (49) follows.

On the other hand, for  $i \neq k$ , we have

$$\frac{\partial u_i}{\partial b_k} = \frac{1}{n_{\text{data}}} a_i \mathbf{t}_i^\top \rho_k a_k \frac{\partial \mathbf{t}_k}{\partial b_k} = \frac{1}{n_{\text{data}}} a_i \mathbf{t}_i^\top \rho_k a_k \mathbf{s}_k,$$

and for  $i = k$ , we obtain

$$\begin{aligned} \frac{\partial u_i}{\partial b_k} &= \frac{1}{n_{\text{data}}} a_i \left( \frac{\partial \mathbf{t}_k}{\partial b_k} \right)^\top (\rho_1 a_1 \mathbf{t}_1 + \dots + \rho_N a_N \mathbf{t}_N) + \frac{1}{n_{\text{data}}} a_k \mathbf{t}_k^\top \rho_k a_k \frac{\partial \mathbf{t}_k}{\partial b_k} \\ &= \frac{1}{n_{\text{data}}} a_i (\mathbf{s}_k)^\top (\rho_1 a_1 \mathbf{t}_1 + \dots + \rho_N a_N \mathbf{t}_N) + \frac{1}{n_{\text{data}}} a_k \mathbf{t}_k^\top \rho_k a_k \mathbf{s}_k. \end{aligned}$$

Combining the above, we obtain  $\frac{\partial \mathbf{u}}{\partial \mathbf{b}}$ , and hence (50) follows.

Finally, noting that  $\mathbf{W}_{i,j}$  is in the  $i$ th row of  $\mathbf{T}$ , for  $i \neq k$ , we obtain

$$\frac{\partial u_k}{\partial \mathbf{W}_{i,j}} = \frac{1}{n_{\text{data}}} a_k \mathbf{t}_k^\top \rho_i a_i \frac{\partial \mathbf{t}_i}{\partial \mathbf{W}_{i,j}} = \frac{1}{n_{\text{data}}} a_k \mathbf{t}_k^\top \rho_i a_i (\mathbf{s}_i \odot \mathbf{x}_j),$$

where  $\mathbf{x}_j$  is the  $j$ th column of  $\mathbf{X}$ . Likewise, for  $i = k$ , we get

$$\begin{aligned} \frac{\partial u_k}{\partial \mathbf{W}_{i,j}} &= \frac{1}{n_{\text{data}}} a_k \left( \frac{\partial \mathbf{t}_k}{\partial \mathbf{W}_{i,j}} \right)^\top (\rho_1 a_1 \mathbf{t}_1 + \dots + \rho_N a_N \mathbf{t}_N) + \frac{1}{n_{\text{data}}} a_k \mathbf{t}_k^\top \rho_k a_k \frac{\partial \mathbf{t}_k}{\partial \mathbf{W}_{i,j}} \\ &= \frac{1}{n_{\text{data}}} a_k (\mathbf{s}_i \odot \mathbf{x}_j)^\top (\rho_1 a_1 \mathbf{t}_1 + \dots + \rho_N a_N \mathbf{t}_N) + \frac{1}{n_{\text{data}}} a_k \mathbf{t}_k^\top \rho_k a_k (\mathbf{s}_i \odot \mathbf{x}_j). \end{aligned}$$

Combining the above, we obtain  $\frac{\partial \mathbf{u}}{\partial \mathbf{W}_{i,j}}$ , thereby arriving at (51). ■

Dataset	JKO-ICNN	SWGF + RealNVP	ProxLearn, weighted	ProxLearn, unweighted
Banana	$0.550 \pm 10^{-2}$	$0.559 \pm 10^{-2}$	$0.551 \pm 10^{-2}$	$0.535 \pm 5 \cdot 10^{-2}$
Diabetes	$0.777 \pm 7 \cdot 10^{-3}$	$0.778 \pm 2 \cdot 10^{-3}$	$0.736 \pm 2 \cdot 10^{-2}$	$0.731 \pm 10^{-2}$
Twonorm	$0.981 \pm 2 \cdot 10^{-4}$	$0.981 \pm 6 \cdot 10^{-4}$	$0.972 \pm 2 \cdot 10^{-3}$	$0.972 \pm 2 \cdot 10^{-3}$

Table 3: Average classification accuracy over 5 runs for three different binary classification problems. Data in the first two columns are reported in [9, Table 1]; the final two columns correspond to our contribution.

## E. Comparisons to Existing Results

Our intent in this paper is to explore designing a new class of algorithms leveraging the connection between the mean field PDE and the Wasserstein proximal operator. Our aim in this work is not to surpass the performance of the carefully engineered existing state-of-the-art per se. Instead, our goal is to explore the possibility of designing a new class of training algorithms by transforming mean field learning from a theoretical tool to a practical algorithm.

As a first study, our numerical results achieved reasonable accuracy compared to the state-of-art even though our proposed meshless proximal algorithm is very different from the existing implementations. In this Section, we compare the numerical performance with existing methods, considering results by Mokrov et al. (2021) [28] and Bonet et al. (2022) [9]. We applied our binary classification algorithm to three datasets also considered in [28] and [9]: the banana, diabetes, and twonorm datasets.

The banana dataset consists of 5300 data points, each with  $n_x = 2$  features, which we rescaled to each lie between 0 and 8. We set  $\beta = 0.05$ , drew our initial weights  $\mathbf{w}$  from  $\text{Unif}([-2, 2]^{n_x})$  and bias  $\mathbf{b}$  from  $\text{Unif}([-0.3, 0.3])$ , and set  $\varrho_0 \equiv \text{Unif}(0, 1000)$ . We ran our code for 3500 iterations to classify this data, splitting the data evenly between test and training data.

The diabetes dataset consists of  $n_x = 8$  features from each of 768 patients. Based on our experimental results, we made the following adjustments from the algorithm presented in the main paper: we redefined  $\beta = 0.65$ ,  $\varrho_0 \equiv \text{Unif}(0, 1000)$ , and drew our initial weights  $\mathbf{w}$  from  $\text{Unif}([-2, 2]^{n_x})$ . We rescaled the data to lie between 0 and 1, and used half of the dataset for training purposes, and the remainder as test data. In this case, we ran our code for  $4.99 \times 10^5$  iterations.

The twonorm dataset consists of 7,400 samples drawn from two different normal distributions, with  $n_x = 20$  features. We again considered 50% of the same as training data and used the remaining 50% as test data, and rescaled the given data by a factor of 8. From our empirical observations, we redefined  $\beta = 1.95$ , and once more drew our initial weights  $\mathbf{w}$  from  $\text{Unif}([-2, 2]^{n_x})$  and set  $\varrho_0 \equiv \text{Unif}(0, 1000)$ . In this case, we performed  $10^4$  proximal recursions in each separate run.

We ran our code five times for each of the three datasets under consideration, and computed "estimate #1" and "estimate #2" in each case, as described in the main paper. These estimates assign each data point a value: negative values predict the label as 0 while positive values predict the label as 1. From these results, we calculated the weighted (from estimate #1) and unweighted (from estimate #2) accuracy in each case, by finding the percentage of predicted test labels that match the actual test labels. The average accuracy over all five runs is reported in Table 3, alongside the results reported in [9, Table 1]. We achieve fairly comparable accuracy to these recent results.